Spatial distribution of carriers in $SrTiO_3$ revealed by photoluminescence dynamics measurements

Hideki Yasuda,[1] Yasuhiro Yamada,[1] Takeshi Tayagaki,[1] and Yoshihiko Kanemitsu[1,2,*]
[1]*Institute for Chemical Research, Kyoto University, Uji, Kyoto 611-0011, Japan*
[2]*Photonics and Electronics Science and Engineering Center, Kyoto University, Kyoto 615-8510, Japan*
(Received 4 September 2008; revised manuscript received 30 October 2008; published 30 December 2008)

We report on the optical determination of the carrier-density profiles near surfaces in $SrTiO_3$ crystals by means of photoluminescence (PL) dynamics measurements. The PL dynamics under band-to-band excitation depends strongly on the excitation photon energy for different optical penetration depths. In nondoped and Ar^+-irradiated $SrTiO_3$ crystals, we evaluate the depth profile of carriers near the surface based on the lifetime of the Auger recombination of electrons originating from oxygen vacancies with photocarriers. Our PL spectroscopy clarifies that in nondoped $SrTiO_3$, the near-surface oxygen-deficient region is a few tens of nanometers in depth.

DOI: 10.1103/PhysRevB.78.233202 PACS number(s): 78.55.−m, 73.50.Gr, 78.47.Cd

Perovskite oxides and their heterostructures have attracted a great deal of attention as new device materials because of their multifunctional properties.[1] With its unique electrical and optical properties, $SrTiO_3$ is a key oxide material, both from a fundamental physics viewpoint and because of its potential for device applications. On the basis of electron doping, $SrTiO_3$ shows multifunctional electrical properties ranging from insulating to semiconducting, metallic, and superconducting.[2–5] The interest in $SrTiO_3$ is further increased by the unique electronic and magnetic properties of the two-dimensional electron-gas system formed at the interfaces between $SrTiO_3$ and other oxides.[6–9] The mechanism of metallic-interface formation is currently under discussion, and two models have been proposed: charge transfer at the oxide interface and oxygen vacancies in the $SrTiO_3$ substrate.[10–14] The development of noncontact probes of the carrier and oxygen-vacancy densities in the microscale region is required, and a quantitative evaluation of the spatial carrier- and defect-density profiles will provide further insights into the physics behind $SrTiO_3$ bulk crystals and heterostructures.

We have reported that Ar^+-irradiated, electron-doped, and highly photoexcited $SrTiO_3$ samples show blue photoluminescence (PL) at room temperature.[15,16] The PL dynamics of $SrTiO_3$ can be explained on the basis of a simple model that includes nonradiative Auger recombination.[16] Because we quantitatively evaluated the Auger recombination rate, whereby the carrier dynamics depends on the carrier density, the analysis of the PL dynamics provides the required information on the carrier density. In addition, the optically monitored region of the sample surface can be controlled by changing the photon energy of the excitation light. Therefore, PL spectroscopy becomes a powerful experimental technique for studying the carrier-density profiles in $SrTiO_3$.

In this Brief Report, we demonstrate that the PL-decay dynamics in nondoped $SrTiO_3$ (STO) and Ar^+-irradiated $SrTiO_3$ (Ar-STO) depends strongly on the excitation photon energy. With an increase in the photon energy, the PL decay time decreases and the PL profile becomes nonexponential. This behavior can be explained by assuming that Auger recombination of electrons originating from oxygen vacancies with photocarriers determines the PL lifetime and that the electron densities near the surface are much higher than those in the bulk crystal. We successfully demonstrate the optical measurement of the depth profile of carriers in the near-surface region of the $SrTiO_3$ samples on the basis of PL dynamics.

We used nondoped $SrTiO_3$ crystals and two types of electron-doped $SrTiO_3$ crystals: $Sr_{0.99}La_{0.01}TiO_3$ and Ar^+-irradiated $SrTiO_3$ (using 300 V accelerated voltage and 3 ml min^{-1} Argon-gas flow for 10 min). Nondoped samples were annealed under oxygen flow for 24 h at 700 K to reduce oxygen vacancies. In the electron-doped samples, electrons were doped by cation substitute (i.e., chemical doping of La ions) and oxygen deficiency (Ar-ion irradiation). All samples were 0.5 mm thick. Time-resolved PL spectra were measured with a time resolution of 40 ps using a streak camera and a monochromator. The excitation light source was an optical parametric amplifier system based on a regenerative amplified mode-locked Ti:sapphire laser with a pulse duration of 150 fs and a repetition rate of 1 kHz. The laser spot size on the sample surface was carefully measured using the knife-edge method. All spectroscopic measurements were carried out at room temperature. The samples used in this work showed broad blue PL peaks at around 2.9 eV. The excitation density n was fixed at 1×10^{18} cm^{-3}, which is low enough to neglect the Auger recombination process of photocarriers, by considering the penetration depth at the photon-excitation energy. We confirmed that the PL dynamics is independent of the excitation intensity under these low-density excitation conditions.

Figure 1(a) shows the PL dynamics monitored at 2.9 eV for STO, La-doped $SrTiO_3$ crystal (La-STO), and Ar-STO samples under 3.26 eV excitation. The excitation energy is close to the band-gap energy of nondoped $SrTiO_3$ of ~3.2 eV and the optical penetration depth at 3.26 eV is large and is about 10 μm. The PL dynamics of nondoped $SrTiO_3$ shows a single exponential decay profile with a lifetime of 50 ns. La-doped $SrTiO_3$ also shows a single exponential decay profile, but the lifetime (2 ns) is much shorter than that of nondoped $SrTiO_3$. In Ar^+-irradiated $SrTiO_3$, we observe two decay components. The first is a fast decay component with a decay time of a few nanoseconds and the second is a slow decay with a decay profile that is quite similar to that of nondoped $SrTiO_3$. It is notable that the fast PL-decay component appears clearly in both electron-doped samples (La-doped and Ar^+-irradiated $SrTiO_3$) under weak laser excitation.

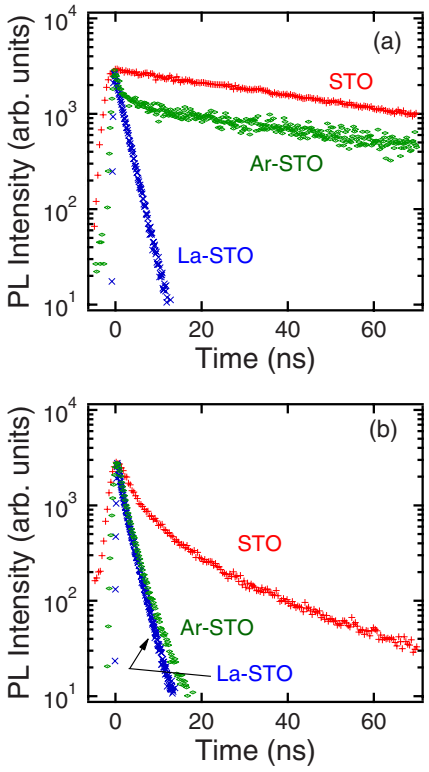

FIG. 1. (Color online) PL dynamics in nondoped, La-doped, and Ar^+-irradiated $SrTiO_3$ (STO, La-STO, and Ar-STO, respectively) samples under excitation at (a) 3.26 and (b) 3.87 eV.

The dynamics of the photocarriers is well described using the following rate equation:[16,17]

$$\frac{dn}{dt} = -An - Bn^2 - Cn^3, \tag{1}$$

where n is the photocarrier density and A, B, and C represent the nonradiative single-carrier-trapping rate, the radiative bimolecular-recombination coefficient, and the nonradiative Auger recombination coefficient, respectively. The bimolecular radiative recombination Bn^2 is negligibly small at room temperature because the PL efficiency is quite low. Previously, we evaluated the Auger coefficient $C=1.3\times10^{-32}$ $cm^6\ s^{-1}$ under high-density photoexcitation.[16] Because the Auger recombination rate is low enough in the low-density excitation condition, the PL dynamics shows a single exponential decay profile [Fig. 1(a)], from which we obtained $A=7.9\times10^6$ s^{-1} for the experimental result using the nondoped $SrTiO_3$ samples.

In La-doped and Ar^+-irradiated $SrTiO_3$ samples, the rapid PL decay is caused by the Auger recombination of electrons originating from oxygen vacancies with photocarriers. When the doped electron density N_e is higher, i.e., $N_e > (A/C)^{1/2}$ $(=2\times10^{19}$ $cm^{-3})$, Auger nonradiative recombination dominates the photocarrier dynamics. In highly doped $SrTiO_3$ such as in $Sr_{0.99}La_{0.01}TiO_3$ crystals, Eq. (1) no longer describes the photocarrier dynamics and should be modified as

$$\frac{dn}{dt} = -An - CN_e^2 n \quad (N_e \gg n). \tag{2}$$

The PL decay time becomes shorter as the doped electron density is increased. In the chemically doped $Sr_{0.99}La_{0.01}TiO_3$ crystals, doped electrons are distributed homogeneously throughout the sample. In this case, the PL decay is a single exponential curve. In contrast, in Ar^+-irradiated $SrTiO_3$, we observe two distinct decay components. Ar^+ irradiation introduces oxygen vacancies near the surface, and the density profile of electrons originating from oxygen vacancies is inhomogeneous in depth.[15,18] We argue that the fast decay component comes from the near-surface metallic layer where Auger recombination of doped electrons with photocarriers is dominant. The slow component comes from the nondoped $SrTiO_3$ substrate. Therefore, the two decay components in the Ar^+-irradiated $SrTiO_3$ crystal originate from two different electron-density regions: the oxygen-deficient metallic layer near the surface and the nondoped insulating substrate. The fast PL-decay component provides quantitative information about the density and spatial profile of carriers in the sample.

Figure 1(b) shows the PL dynamics in three samples under an excitation of 3.87 eV. The excitation energy is well above the band-gap energy of the nondoped samples, and the penetration depth at 3.87 eV is very small and is about 40 nm. Thus, the photocarriers are generated in the near-surface region, and the PL dynamics is strongly affected by oxygen vacancies in the near-surface region. Nondoped $SrTiO_3$ shows nonexponential decay that is faster than that under an excitation of 3.26 eV. Even in the nominally nondoped sample, defects producing electron carriers are inevitably introduced, especially very close to the surface.[19] In contrast, in La-doped $SrTiO_3$, the absence of any significant dependence of the PL decay time on the excitation energy also clearly supports the spatially homogeneous distribution of doped electrons. Moreover, Ar^+-irradiated $SrTiO_3$ shows only the fast decay component; the slow decay component disappears. This implies that the PL dynamics is determined by the near-surface oxygen-deficient metallic layer under high-energy excitation. Our findings show that the spatial distributions of electron carriers in $SrTiO_3$ crystals can be estimated from the photon-energy dependence of the PL dynamics.

First, we discuss the spatial distribution of electron carriers originating from oxygen vacancies in Ar^+-irradiated $SrTiO_3$ composed of the metallic near-surface layer and insulating nondoped substrate. In Fig. 2(a) we show the excitation photon-energy dependence of the intensity ratio of the fast decay components. The optical penetration depth, estimated from the reflection spectra from Ref. 20, is also shown. Here, we approximately describe the PL-decay curves shown in Fig. 1 using two exponential functions and fix the decay time of the slow decay component to 50 ns. With an increase in the excitation energy, the optical penetration depth decreases and the photocarriers are generated in the near-surface region. Therefore, the PL from the near-surface metallic layer increases and that from the insulating substrate decreases.

To evaluate the electron-carrier distribution near the surface quantitatively, we focus on the fast PL dynamics. Figure 2(b) shows the PL-decay curves in Ar^+-irradiated $SrTiO_3$ samples under excitation of 3.76, 3.87, and 4.00 eV. To study the spatial distribution of the carrier density, we assumed

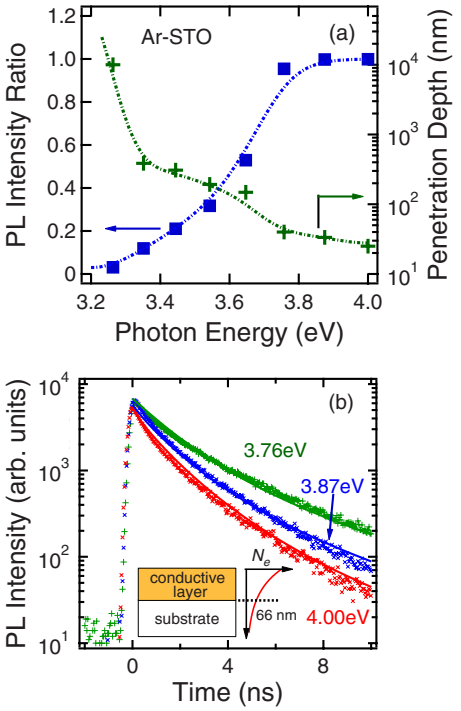

FIG. 2. (Color online) (a) PL intensities of the fast decay component in the Ar^+-irradiated $SrTiO_3$ (square). The crosses show the optical penetration depth obtained from Ref. 20. (b) PL dynamics in Ar^+-irradiated $SrTiO_3$ samples under 3.76, 3.87, and 4.00 eV excitation. The solid lines show the fitting results obtained by assuming an exponential distribution of the carriers. The inset illustrates the metallic layer formed at the surface of Ar^+-irradiated $SrTiO_3$ crystals.

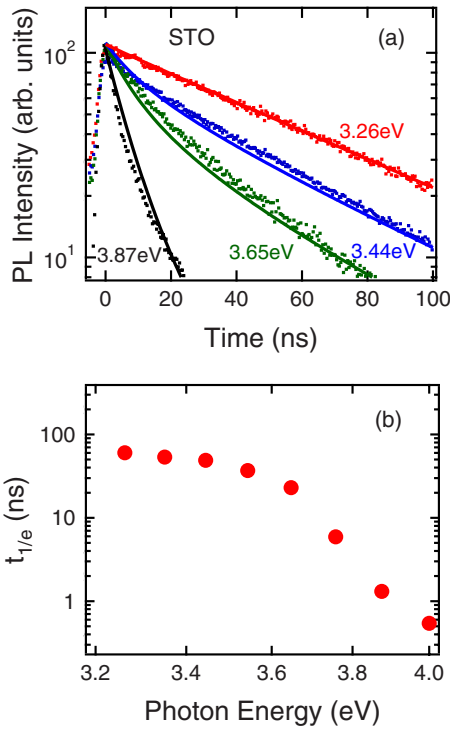

FIG. 3. (Color online) (a) PL dynamics in nondoped $SrTiO_3$ under excitation at 3.26, 3.44, 3.65, and 3.87 eV. (b) Photon-energy dependence of the decay time measured under excitation of $n = 10^{18}$ cm^{-3}.

the exponential spatial profile as a trial function $N_e(z) = N_0 \exp(-\beta z)$, where $1/\beta$ is the depth of the carrier distribution. The temporal variation in the luminescence is expressed as

$$I(t) \propto B \int_0^\infty N_e(z) n(z,t) dz, \tag{3}$$

where $n(z,t)$ is given by Eq. (2) and $n(z,0) = n_0 \exp(-\alpha z)$ and $1/\alpha$ is the optical penetration depth. Here we assumed that the values of A, B, and C coefficients are independent of the densities of oxygen deficiencies and carriers. The fitting results of Eq. (3) are shown in Fig. 2(b) as the solid lines, reproducing the experimental results rather well. The best-fit parameters are $1/\beta = 66$ nm and $N_0 = 2.4 \times 10^{20}$ cm^{-3}. These results are schematically illustrated in the inset of Fig. 2(b). Therefore, we conclude that in Ar^+-irradiated $SrTiO_3$, the electron carriers doped by oxygen deficiencies are distributed in an exponential decay profile from the surface. In the present experiments and analyses, the spatial resolution is about 10 nm, which is determined by the penetration depth of incident UV light. The metallic near-surface layer is estimated to be ~60 nm deep, which is consistent with the transmission electron microscopy observations in Ref. 15.

We also evaluate the spatial profile of electrons originating from oxygen vacancies in nondoped $SrTiO_3$. Figure 3(a) shows the PL dynamics in nondoped $SrTiO_3$ under excitation at 3.26, 3.44, 3.65, and 3.87 eV. The PL-decay dynamics strongly depends on the excitation photon energy. The PL dynamics under 3.26 eV excitation shows a single exponential decay profile with a lifetime of 50 ns. With an increase in the photon energy, the PL shows a nonexponential profile and the PL decay time becomes shorter. We define the PL decay time $t_{1/e}$ using $I(t_{1/e}) = I(0)/e$ and plot the decay time as a function of the photon energy at the low-excitation photon density of 1×10^{18} cm^{-3} in Fig. 3(b). The decay time abruptly decreases when the photon energy exceeds 3.5 eV. As discussed for the Ar^+-irradiated $SrTiO_3$ samples, this photon-energy dependence comes from the inhomogeneous distribution of electron carriers as a function of depth and suggests the formation of an oxygen-deficient region near the surface, even in nondoped $SrTiO_3$ samples.

The PL dynamics in $SrTiO_3$ samples is sensitive to the photocarrier density n as described by Eq. (1). Therefore, to evaluate the density of electrons from the oxygen vacancies in the near-surface region and the Auger recombination rate of photocarriers, it is necessary to measure the PL decay time as a function of the excitation intensity. Figure 4 shows the photocarrier-density dependence of the decay time at different excitation photon energies. At high densities $n \gtrsim 10^{19}$ cm^{-3}, the decay time shows a rapid decrease proportional to $1/n^2$, indicating the appearance of the Auger recombination of the photocarriers.[16] Under low-density excitation, below the solid line in Fig. 4, the decay time remains almost constant for each excitation photon energy. Thus, the electron-density profile in the near-surface region, $N_e(z)$, is determined by the photon-energy dependence of the

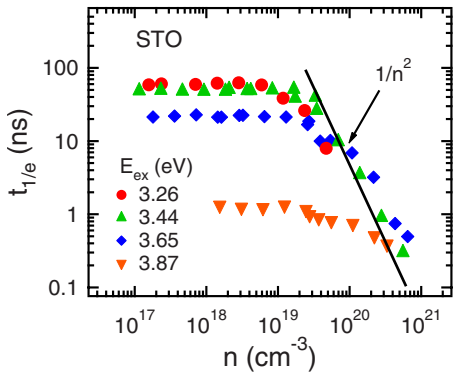

FIG. 4. (Color online) Photocarrier-density dependence of the PL decay times in nondoped $SrTiO_3$ for different photon-excitation energies.

PL-decay profile at the low photocarrier density of $n=1\times10^{18}$ cm^{-3}.

By comparing Figs. 2(b) and 3(a), we assume that the oxygen-deficient layer is formed near the surface of nondoped $SrTiO_3$ and that the electron-density profile is exponential in depth similar to that for Ar^+-irradiated $SrTiO_3$. Using Eq. (3), we obtain the exponential carrier profile $N_e(z)=N_0\exp(-\beta z)$, where $N_0=8\times10^{19}$ cm^{-3} and $1/\beta=16$ nm. The fitting results reproduce the experimental results fairly well, as shown by the solid lines in Fig. 3(a). This means that very thin and electron-rich layers are formed near the surface, even in nondoped $SrTiO_3$. The electron density is low and the thickness of the layer is very thin compared to Ar^+-irradiated $SrTiO_3$. However, the estimated surface carrier density seems to be high for the nondoped $SrTiO_3$ because it is known that the nondoped $SrTiO_3$ substrate is insulator.

In the above discussion, oxygen vacancies produce electron carriers and the Auger recombination of electrons originating from oxygen vacancies with photocarriers determines the PL-decay dynamics. We assumed that the value of A coefficient is independent of the densities of oxygen deficiencies and carriers. However, highly dense oxygen vacancies will affect the carrier-trapping coefficient A in Eq. (1). In fact, in nondoped $SrTiO_3$, the electron density obtained is close to the Auger-limit density $(A/C)^{1/2}$, in which case an increase in the carrier-trapping coefficient will affect the PL-decay dynamics. In such cases, the excited-photon-energy dependence of the PL-decay dynamics means the spatial distribution of the carrier-trapping rate. We point out that an increase in the A coefficient reduce the estimated carrier density in nondoped samples and speculate that the insulating behavior of nondoped $SrTiO_3$ originates from the increase in the carrier-trapping rate near the surface. In both cases of the carrier-trapping and Auger recombination limits, the appearance of the photon-energy dependence of the PL dynamics reflects the depth profiles of the oxygen-vacancy density and clearly shows the existence of the oxygen-deficient surface layer.

In conclusion, the PL dynamics under band-to-band excitation depends strongly on the excitation photon energy. The excitation-energy-dependent PL dynamics can be explained by the Auger recombination process of electrons originating from oxygen vacancies with photocarriers. We have clarified that in nondoped $SrTiO_3$, an oxygen-deficient near-surface layer exists with a depth of a few tens of nanometers.

The authors thank T. Terashima for providing the Ar^+-irradiated $SrTiO_3$ samples. Part of this study was supported by the MEXT Joint Project of Chemical Synthesis Core Research Institutions and Kyoto University Global Center of Excellence (G-COE) program from MEXT.

*Corresponding author; kanemitu@scl.kyoto-u.ac.jp

[1] W. Eerenstein, N. D. Mathur, and J. F. Scott, Nature (London) **442**, 759 (2006).
[2] H. P. R. Frederikse, W. R. Thurber, and W. R. Hosler, Phys. Rev. **134**, A442 (1964).
[3] O. N. Tufte and P. W. Chapman, Phys. Rev. **155**, 796 (1967).
[4] J. F. Schooley, W. R. Hosler, and M. L. Cohen, Phys. Rev. Lett. **12**, 474 (1964).
[5] H. Suzuki, H. Bando, Y. Ootuka, I. H. Inoue, T. Yamamoto, K. Takahashi, and Y. Nishihara, J. Phys. Soc. Jpn. **65**, 1529 (1996).
[6] A. Ohtomo and H. Y. Hwang, Nature (London) **427**, 423 (2004).
[7] A. Tsukazaki, A. Ohtomo, T. Kita, Y. Ohno, H. Ohno, and M. Kawasaki, Science **315**, 1388 (2007).
[8] A. Brinkman, M. Huijben, M. Van Zalk, J. Huijben, U. Zietler, J. C. Maan, W. G. Van der Wiel, G. Rijnders, D. H. A. Blank, and H. Hilgenkamp, Nature Mater. **6**, 493 (2007).
[9] N. Reyren, S. Thiel, A. D. Cavigla, L. Koukoutis, G. Hammerl, C. Richter, C. W. Schneider, T. Kopp, A. S. Rüetschi, D. Jaccard, M. Gabay, D. A. Muller, J. M. Triscone, and J. Mannhart, Science **317**, 1196 (2007).
[10] N. Nakagawa, H. Y. Hwang, and D. Muller, Nature Mater. **5**, 204 (2006).
[11] G. Herranz, M. Basletic, M. Bibes, C. Carrétéro, E. Tafra, E. Jacquet, K. Bouzehouane, C. Deranolt, A. Hamzić, J. M. Broto, A. Barthélémy, and A. Fert, Phys. Rev. Lett. **98**, 216803 (2007).
[12] W. Siemons, G. Koster, H. Yamamoto, W. A. Harrison, G. Lucovsky, T. H. Geballe, D. H. A. Blank, and M. R. Beasley, Phys. Rev. Lett. **98**, 196802 (2007).
[13] A. Kalabukhov, R. Gunnarsson, J. Borjesson, E. Olsson, T. Claeson, and D. Winkler, Phys. Rev. B **75**, 121404(R) (2007).
[14] M. Basletic, J.-L. Maurice, C. Carretero, G. Herranz, O. Copie, M. Bibes, E. Jacwuet, K. Bouzehouane, S. Fusil, and A. Barthelemy, Nature Mater. **7**, 621 (2008).
[15] D. Kan, T. Terashima, R. Kanda, A. Masuno, K. Tanaka, S. Chu, H. Kan, A. Ishizumi, Y. Kanemitsu, Y. Shimakawa, and M. Takano, Nature Mater. **4**, 816 (2005).
[16] H. Yasuda and Y. Kanemitsu, Phys. Rev. B **77**, 193202 (2008).
[17] P. T. Landsberg, *Recombination in Semiconductors* (Cambridge University Press, Cambridge, 1991).
[18] V. E. Henrich, G. Dresselhaus, and H. J. Zeiger, Phys. Rev. B **17**, 4908 (1978).
[19] K. Szot, W. Speier, R. Carius, U. Zastrow, and W. Beyer, Phys. Rev. Lett. **88**, 075508 (2002).
[20] M. Cardona, Phys. Rev. **140**, A651 (1965).